Contribution to the Diffuse Radio Background from Extragalactic Radio Sources

by

Tessa Vernstrom

Bachelor of Scienece:Astrophysics, University of Minnesota, 2008

A THESIS SUBMITTED IN PARTIAL FULFILLMENT
OF THE REQUIREMENTS FOR THE DEGREE OF

Master of Astronomy

in

THE FACULTY OF GRADUATE STUDIES
(Astronomy)

The University Of British Columbia
(Vancouver)

August 2011

Abstract

We examine the brightness of the Cosmic Radio Background (CRB) by comparing the contribution from individual source counts to absolute measurements. We use a compilation of radio counts to estimate the contribution of detected sources to the CRB in several different frequency bands. Using a Monte Carlo Markov Chain technique, we estimate the brightness values and uncertainties, paying attention to various sources of systematic error. At ν = 150 MHz, 325 MHz, 408 MHz, 610 MHz, 1.4 GHz, 4.8 GHz, and 8.4 GHz our calculated contributions to the background sky temperature are 18, 2.8, 1.6, 0.71, 0.11, 0.0032, 0.0059 K, respectively. We then compare our results to absolute measurements from the ARCADE 2 experiment. If the ARCADE 2 measurements are correct and come from sources, then there must be an additional population of radio galaxies, fainter than where current data are probing. More specifically, the Euclidean-normalized counts at 1.4 GHz have to have an additional bump below about 10 μJy. We present preliminary results of investigating this new population by use of signal stacking. By stacking onto a very deep 1.4 GHz radio map at source positions determined in the infrared and optical we hope to be able to see evidence of this population that would be too faint to be seen individually. Results are currently inconclusive. Future work will consist of modelling radio luminosity functions and new observations with the Extended VLA to continue to search for what may be causing this excess emission.

Table of Contents

List of Tables

List of Figures

Acknowledgments

Thanks to both of my advisors Douglas Scott and Jasper Wall. And to NSERC for the funding.

Chapter 1

Introduction

Investigating what sources make up the diffuse extragalactic background over a wide range of wavelengths can help us to understand the different physical mechanisms which govern the generation and transport of energy over cosmic time (e.g Longair and Sunyaev 39, Ressell and Turner 53). Much effort has gone into resolving the sources which comprise the background at γ-ray, X-ray, optical, and infra-red wavelengths (e.g. 7, 28, 36, 40). However, the radio part of the spectrum has received far less attention. While there have been many radio surveys and compilations of source counts done over the years, there have been only a few attempts at using these to obtain estimates of the background temperature (14, 38, 51, 63). With the advent of new absolute measurements of the radio background, coupled with radio source counts to ever increasing depths, the topic has undergone something of a revival.

1.1 The Cosmic Background

Most of the electromagnetic energy of the universe is in the cosmic microwave background radiation left over from the hot big bang. It has a nearly perfect $\sim$ 2.73 K blackbody spectrum peaking at $\lambda \sim 1\,\mathrm{mm}$. The strong UV/optical peak is primarily thermal emission from stars, supplemented by a smaller contribution of thermal and nonthermal emission from the active galactic nuclei (AGN) in Seyfert galaxies and quasars. Most of the comparably strong cosmic infrared background

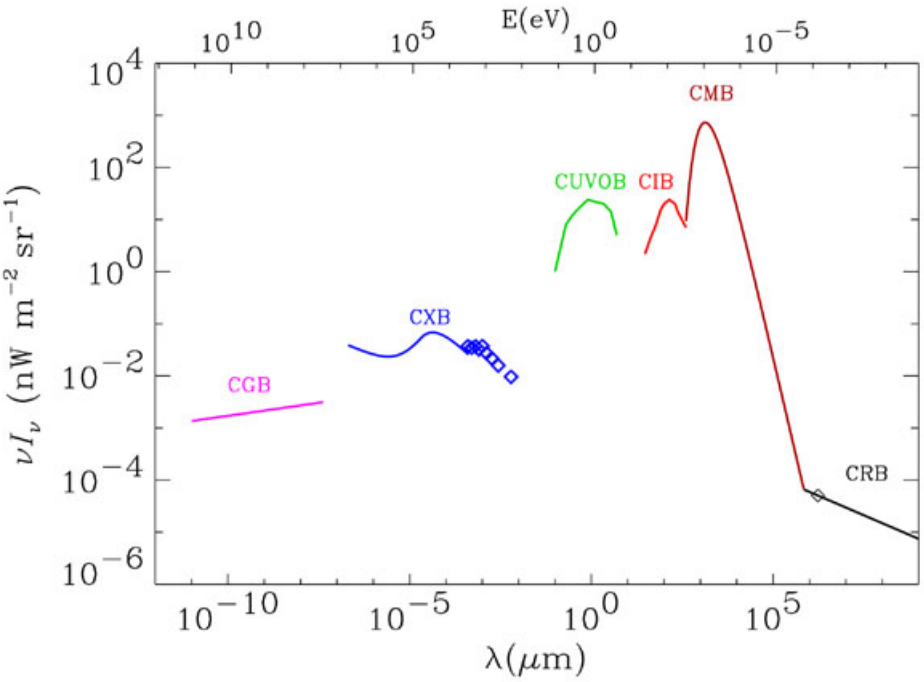

Figure 1.1: The Cosmic Backgrounds: the electromagnetic spectrum of the universe. The brightness per logarithmic frequency (or wavelength) interval is shown as a function of the logarithm of the wavelength, so the highest peaks correspond to the most energetic spectral ranges.

is thermal re-emission from interstellar dust heated by absorbing that UV/optical radiation. The cosmic X-ray and gamma-ray backgrounds are mixtures of non-thermal emission (e.g., synchrotron radiation or inverse-Compton scattering) from high-energy particles accelerated by AGN and thermal emission from very hot gas (e.g., gas in clusters of galaxies). By comparison, the cosmic radio-source background is extremely weak. Although they may be energetically insignificant, radio sources do trace most phenomena that are detectable in other portions of the electromagnetic spectrum, and modern radio telescopes are sensitive enough to detect extremely faint radio emission. The cosmic radio background is a combination of emission from discrete sources and a component from the CMB blackbody. Since the CMB blackbody is well measured, it is the component from discrete radio

sources that allows room for further study.

1.2 Radio Source Counts

Source counts, corresponding to the surface density of sources as a function of flux density, can be directly compiled from any complete sample, without any additional data. Because flux density is a function of both redshift and luminosity, source counts are the first probes into the behaviour of galaxy evolution.

Source counts can come in different forms, the most basic being the cumulative (or integrated) source count, $N(>S)$ (Fig. 1.2, top panel), describing the expected number of sources per unit area above a given flux density. Because of its cumulative nature, consecutive data points are not statistically independent of each other, which can be problematic, especially in the corresponding error analysis. The differential form of the source count (Fig. 1.2, central panel), which describes the number of sources per unit area in a given flux bin ($\Delta N/\Delta S$), avoids the problem of dependence of consecutive values.

Because the differential source count is generally very steep, possibly hiding some important features, it is customary to represent it relative to the count of uniformly distributed sources in a flat, non-evolving Euclidean Universe, where

$$\Delta N_0 = K_\nu S_\nu^{-3/2}. \tag{1.1}$$

Here the arbitrary constant K_ν usually taken from the number density of sources with flux-densities above 1 Jy. This is the relative differential source count $\Delta N/\Delta N_0$ (Fig. 1.2, bottom panel).

Recently a paper by Gervasi et al. [21] attempted to obtain fits to the source count data across a range of frequencies from ν = 150 to 8440 MHz. From their fits, which ranged from 1 μJy to 100 Jy, they were able to integrate the source counts to obtain an estimate of the sky brightness temperature contribution at each of the frequencies. They determined a power-law sky brightness temperature dependency on frequency with a spectral index of –2.7, which is in agreement with the frequency dependence of the flux density emitted by synchrotron dominated steep-spectrum radio sources. These estimates were used to interpret absolute measurements of the radio sky brightness by the TRIS experiment [69].

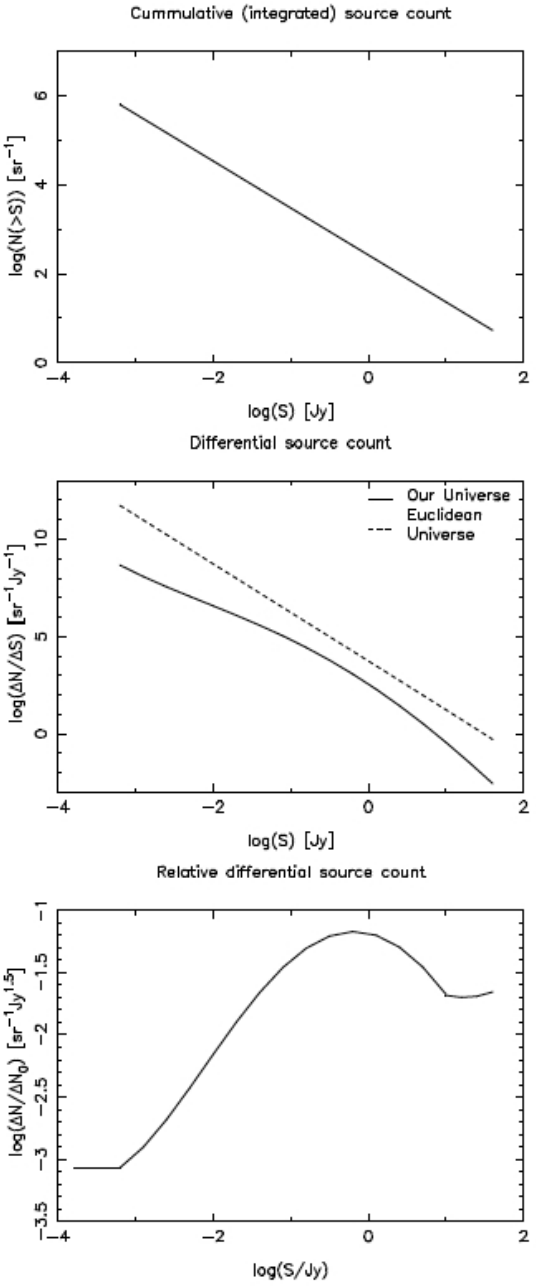

Figure 1.2: 1.4 GHz source counts in cumulative $N(> S)$ (top), differential $\Delta N/\Delta S$ (center) and relative $\Delta N/\Delta N_0$ differential (bottom) forms. The curves represent counts derived from sources in the NVSS (Condon et al., 1998) and Phoenix [30] surveys.

1.3 ARCADE 2

More recently the results of the 2006 ARCADE 2 balloon-borne experiment were released [16, 57]. This instrument provided absolute measurements of the sky temperature at 3, 8, 10, 30, and 90 GHz. These results showed a measured temperature of the radio background about 5 times greater than that currently determined from radio source counts, with the most notable excess of emission being detected at 3 GHz. Since most systematic effects explaining this emission were ruled out, we are left with the question of whether it could be caused by some previously unknown source of extragalactic emission.

It was suggested by in the ARCADE 2 results paper Seiffert et al. [57] that this excess emission may be coming from the sub-μJy range. One might imagine an unknown population of discrete sources existing below the flux limit of current surveys. This issue was further examined by Singal et al. [60]. Taking into account that a class of low flux sources must extend to $\sim 10^{-2}\mu$Jy (at 1.4 GHz), they concluded that this emission could primarily be coming from ordinary star-forming galaxies at $z > 1$ if the radio to far-infrared observed flux ratio increases with redshift.

1.4 Structure of the thesis

Before looking for radical causes of this emission, it is worth reexamining the observed radio source data to see if the ARCADE 2 result really does differ from what is expected. To do this we derive new estimates of the source-integrated CRB at various frequencies and derive formal error estimates for each. In Chapter 2 we describe the source count data used, together with our procedure and results for fitting the observed radio data. In Chapter 3 we present our estimates for the background sky temperature contributions and the analysis of the uncertainties associated with these estimates, as well as a comparison of our results to those obtained by the ARCADE 2 and TRIS collaborations. In Chapter 4 we discuss different options for investigating causes of the excess emission. The main bulk of work of this thesis, with the exception of Section 4.2, has been published in the Monthly Notices of the Royal Astronomical Society, Volume 415, Issue 4, pp. 3641–3648 [62].

Chapter 2

The Radio Counts and Their Fits

2.1 The Data Set

Radio source counts at lower frequencies have been available since the 1960s. There are many compilations of radio source counts available, particularly in the last decade e.g. [4, 18, 30, 52]. More recently deep continuum surveys at higher frequencies have become available, and with the use of newer technologies, have dramatically increased the amount and quality of data. The data used in this paper are from continuum surveys carried out from 1979 to 2009 (see [11, 61]). We used source count distributions from 150 MHz to 8400 MHz, with the individual frequencies covered being ν = 150 MHz, 325 MHz, 408 MHz, 610 MHz, 1.4 GHz, 4.8 GHz and 8.4 GHz. References for all number counts used can be found in Table 2.1.

2.2 The Number Counts Fit

For fitting the source count data we opted to use a fifth order polynomial. A third order polynomial was used in source count fitting by Katgert et al. [34] and a sixth order polynomial fit to the 1.4 GHz data was used by Hopkins et al. [30], while Gervasi et al. [21] used simple power-law fitting. Polynomial fits are simpler than some other choices of function, but still allow for fitting of different features in the data, such as the upturn at the low flux end seen at some of the frequencies

Table 2.1: References for the extragalactic radio count data compilation

Frequency	References
150 MHz	Hales et al. [27], McGilchrist et al. [42].
325 MHz	Oort et al. [46], Owen and Morrison [48], Sirothia et al. [61].
408 MHz	Benn et al. [2], Grueff [24], Robertson [55].
610 MHz	Bondi et al. [5], Garn et al. [20], Ibar et al. [31]. Katgert [33], Moss et al. [45].
1.4 GHz	Bondi et al. [6], Bridle et al. [8], Ciliegi et al. [9]; Fomalont et al. [19], Gruppioni et al. [25]; Hopkins et al. [30], Ibar et al. [31], Miller et al. [43], Mitchell and Condon [44]: Owen and Morrison [48], Richards [54], Seymour et al. [59], White et al. [64].
4.8 GHz	Altschuler [1], Donnelly et al. [13], Fomalont et al. [17], Gregory et al. [23] ; Kuehr et al. [35], Pauliny-Toth et al. [49], Wrobel and Krause [68].
8.4 GHz	Fomalont et al. [18], Henkel and Partridge [29], Windhorst et al. [67].

(where we note that an additional sub-mJy peak could make a substantial contribution to the background). We chose a fifth order polynomial as it is high enough order to account for the features seen in the 1.4 GHz data. Going to higher orders creates unnecessary extra parameters while not improving the χ^2 by a significant amount. Our empirical fits are performed on the Euclidean-normalized counts, i.e. $F(S) = S^{2.5}(dN/dS)$, with S being the flux density in Jy, using the polynomial with parameters

$$F(S) = A_0 + A_1 S + A_2 S^2 + A_3 S^3 + A_4 S^4 + A_5 S^5. \tag{2.1}$$

The fitting is initially performed using a χ^2 minimization routine. The coefficients given by the χ^2 minima are then used as starting points in a Monte Carlo Markov Chain, or MCMC approach [37], which is used to refine the fits and obtain estimates of uncertainty. More details on the MCMC method can be found in Section 3.2. The best fit values for all the parameters at each of the frequency bands can be found in Table 2.2 along with χ^2 values for each fit. The data and the best fit lines are plotted in Fig. 2.1, which shows the Euclidean normalized data, as well as the S^2 normalized results. These $S^2(dN/dS)$ (surface brightness per logarithmic interval in flux density) plots are included to show where the peak contributions to the background arises. The right-hand panels in Fig. 2.1 show that the bulk of the background comes from relatively bright radio sources, with $S \sim 1$ Jy at the lowest

Table 2.2: χ^2 values for best fits at each of the frequencies

ν MHz	χ^2	Degrees of Freedom	A_0	A_1	A_2	A_3	A_4	A_5
150	68	45	6.58	0.36	−0.65	−0.19	0.26	0.099
325	59	34	5.17	0.029	−0.11	0.36	0.17	0.20
408	66	44	4.13	0.13	−0.34	−0.003	0.035	0.01
610	75	59	3.02	0.71	0.97	0.91	0.28	0.028
1400	4230	196	2.53	−0.052	−0.020	0.051	0.010	−0.0013
4800	32	47	1.95	−0.076	−0.15	0.020	0.0029	−0.00079
8400	41	29	0.79	−0.10	−0.23	−0.051	−0.019	−0.0029

frequencies to tens of mJy at the highest frequencies. But there is a significant, and still poorly characterized, contribution from much fainter sources.

Table 2.2 shows that the χ^2 values of the fits are generally good, with all but one of the reduced χ^2 values being below 2. The exception is for the 1.4 GHz data set, with a χ^2 of over 20 per degree of freedom. To obtain anything like a reasonable χ^2 we would have to increase the errors by a factor of four. It is worrisome that the 1.4 GHz compilation is the one with the most available data. As can be seen in the plot, there are many data points that are inconsistent with each other, even with the relatively large error bars.

There are clearly systematic differences between different surveys at 1.4 GHz, particularly at the faint end. In the μJy range it is difficult to obtain reliable counts, as this range is close to the natural confusion limit of most radio surveys ([10, 66]) and hence the level of incompleteness may be incorrectly estimated in some surveys. Moreover, at the bright end there are significant and systematic sources of error introduced when attempting to correct for source extension and surface brightness limitations (see discussion in Singal et al. [60]). In addition to these effects, sampling variance (enhanced by source clustering) can lead to differences in counts for small fields. All of these systematic effects make it difficult to assess robustly the uncertainties in the derived CRB, as we discuss in the next section.

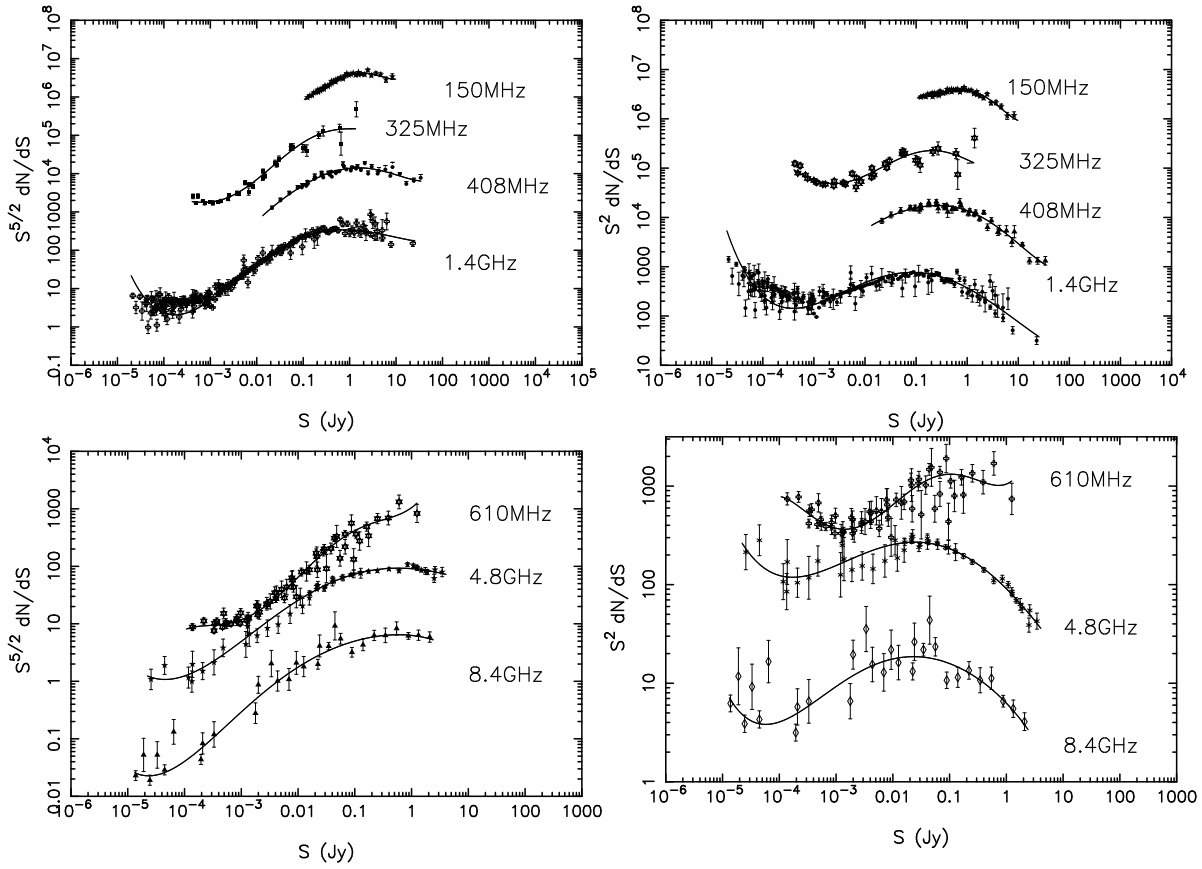

Figure 2.1: Left: Differential source counts Euclidean normalized and multiplied by c, with c = 1000,100, 10, 1, 1, 1, and 0.1 for ν = 150, 325, 408, 610, 1400, 4800, and 8400 MHz, respectively. Right: S^2 normalization to show where the contribution to the sky brightness temperature is largest. The counts are a compilation from many different surveys, listed in Table 2.1. Solid lines are best fit polynomials.

Chapter 3

Contribution to Sky Brightness Temperature

3.1 Integration of Radio Counts

We integrate best-fit polynomials to obtain the contribution from the sources to the sky brightness. To do this we integrate the function $S(dN/dS)$ for each data set only in the range where data are available. We make this conservative choice to avoid extrapolating at the very low and high flux density ends. Because of this our estimates of the sky brightness should be seen as lower limits. Thus to estimate the intensity we integrate

$$I(\nu) = \int_{S_{\min}}^{S_{\max}} \frac{dN}{dS}(\nu) \cdot S \, dS, \tag{3.1}$$

where $S_{\min}$ and $S_{\max}$ are different for each frequency. Once the intensity is determined we use the Rayleigh-Jeans approximation to convert it to a brightness temperature,

$$T(\nu) = I(\nu)\frac{\lambda^2}{2k}, \tag{3.2}$$

where k is the Boltzmann constant. The results from the integration at each of the seven frequencies are listed in Table 3.1.

After obtaining these conservative estimates we next investigate the effect of reasonable extrapolations on the results, with the limits of integration broadened

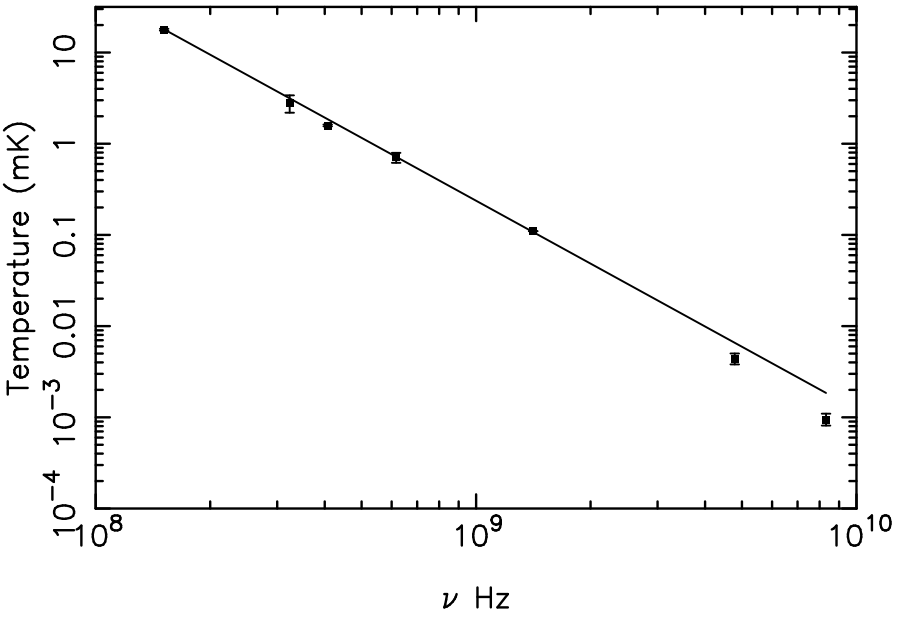

Figure 3.1: Integration results and best fit power law from Equation 3.3.

Table 3.1: Values of the integrated sky brightness and temperature contribution from radio source counts for different frequency bands. The uncertainties are 1σ limits determined from Markov chain polynomial fits to the data. The high and low extrapolations are discussed in the text.

ν	νI_ν	T	δT	Extrapolated T	
				High	Low
MHz	W m^{-2} sr^{-1}	mK	mK	mK	mK
150	1.8×10^{-14}	17800	300	29400	18100
325	2.1×10^{-14}	2800	600	5040	3100
408	2.9×10^{-14}	1600	30	3000	1850
610	4.2×10^{-14}	710	90	1200	740
1400	7.5×10^{-14}	110	20	180	110
4800	8.0×10^{-14}	3.2	0.2	10.8	6.7
8400	9.6×10^{-14}	0.59	0.05	3.0	1.9

to 10^{-6} Jy and 10^{2} Jy for $S_{\rm min}$ and $S_{\rm max}$, respectively. The 1.4 GHz data set has the most extensive coverage across the flux density range. For this reason, we manually extrapolate the curve for the 1.4 GHz data set and integrate to get a new estimate for the background temperature. To extend the limits of integration for the 1.4 GHz data the end behaviour of the polynomial is constrained with the assumption that the counts fall off beyond the low-intensity end of the data. Artificial points are added in this region and their positions varied until a reasonable fit to the data is achieved. This procedure is repeated with both a steep and shallow roll-off, to obtain high and low background estimates. These slopes are chosen to be the most reasonable steep and shallow estimates, with the χ^2s being a factor of 5 and 7 greater than the best fit to the data alone. The best fits for the extrapolations can be seen in Fig. 3.2. The higher estimate could have been allowed to have an even shallower slope, therefore allowing for an even higher background estimate; however anything much shallower than the chosen fit would have χ^2 values several times larger again. This fact makes any shallower fits an unreasonable choice. The steep slope estimate for the 1.4 GHz data ends up giving nearly the same result for the background temperature as the unextrapolated estimate. This is because the unextrapolated estimate has a rising low-intensity tail (Fig. 1), while the extrapolated estimate (Fig. 3.2) has limits of integration extended with the roll-off procedure, whose end behaviour is controlled to produce a steep down turn beyond the available data.

From our conservative estimate of the 1.4 GHz background a power-law is fit to the temperatures. This takes the form of

$$T(\nu) = A\left(\frac{\nu}{1.4\,\mathrm{GHz}}\right)^{\beta}\ , \tag{3.3}$$

where A is the power-law amplitude, and β the index. We set A to the 1.4 GHz value of 0.110 K, while Monte Carlo Markov Chains (section 3.2) were used to find the best value of β = –2.28 $\pm$ 0.1. The results of this power-law fit can be seen in Fig. 3.1. The fit is high for the two highest frequency points, primarily as a result of the 1.4 GHz data, which has the most flux density coverage and most available data. It should be noted that this is just a phenomenological fit; we see little merit in adopting a more complex model such as a broken power-law just to

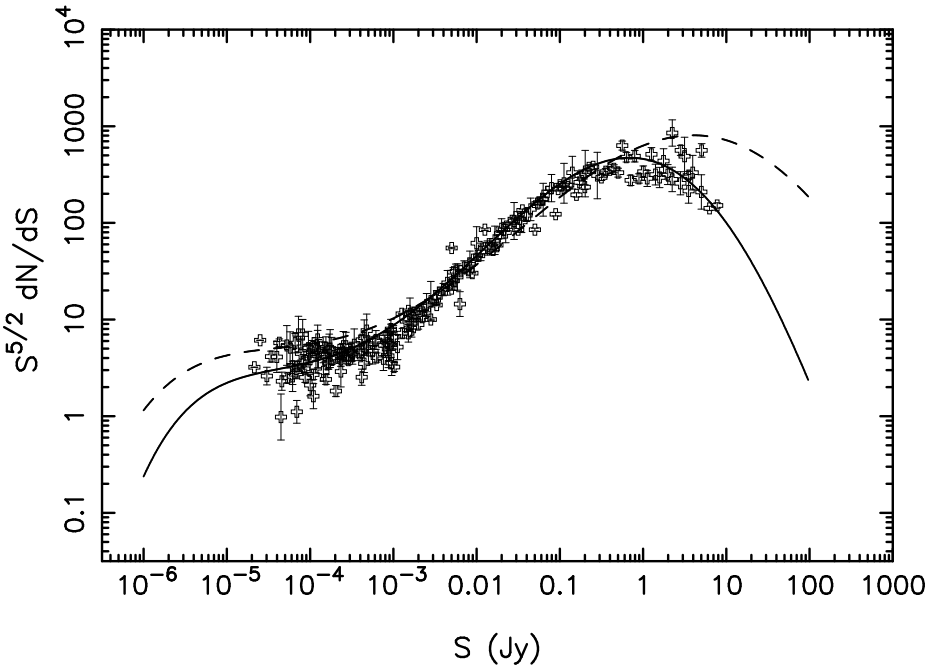

Figure 3.2: 1.4 GHz data set with fit lines showing extrapolations out to 10^{-6} and 10^2Jy. The solid and dashed lines show estimates for steeper and shallower slopes, respectively.

satisfy two extreme data points, particularly when this power law is only used to obtain extrapolation estimates.

With the high and low extrapolation estimates from the 1.4 GHz data, we use Equation 3.3 to obtain estimates for the other frequencies. The results of the extrapolated estimates are given in Table 3.1. As even these reasonable extrapolations can change the background estimates by about a factor of two, it is clearly important to push counts at all frequencies to fainter levels.

3.2 Uncertainty – Monte Carlo Markov Chains

To investigate the uncertainties thoroughly, we carry out our fits with Monte Carlo Markov chains for each of the data sets, using CosmoMC [37] as a generic MCMC sampler. The χ^2 function is sampled for each set using the polynomial in Equation 2.1 which is then fed to the sampler to locate the χ^2 minimum. Each of the six pa-

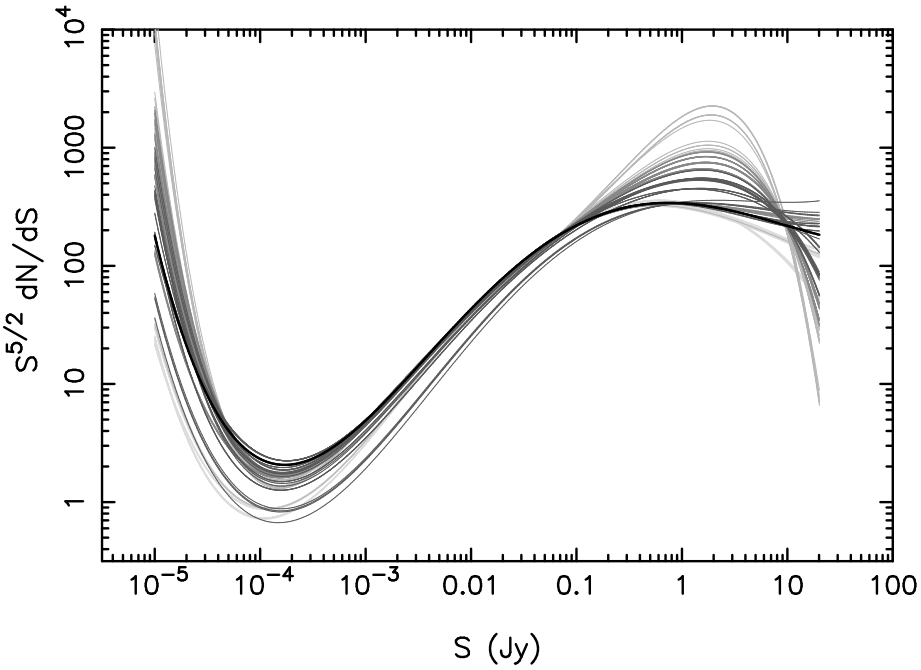

Figure 3.3: 100 Markov Chain polynomial fits generated for the 1.4 GHz data set. Greyscale indicates relative probability, with the solid black line being the best fit curve.

rameters of the polynomials are varied for each step of the chain and the chains are run with 500,000 steps. CosmoMC generates statistics for the chains, including the minimum χ^2, the best fit values for each of the parameters, and their uncertainties. As an example, Fig. 3.3 shows different polynomial fits tested by the MCMC and their relative probability for the 1.4 GHz data set.

Histograms of the chain values for the background temperature are shown in Fig. 3.4. From the width of these histograms we are able to measure the uncertainty in our estimates for the background temperature, taken here as the 68 percent area values, fully accounting for the correlations among the parameters in the polynomial fits. The 1σ uncertainties are listed in Table 3.1.

Most of the histograms are fairly Gaussian, which is a reflection of the quality of the data. Frequencies with good data around the peak contribution (in the right-hand panels of Fig. 2.1) tend to have well-constrained background temperature

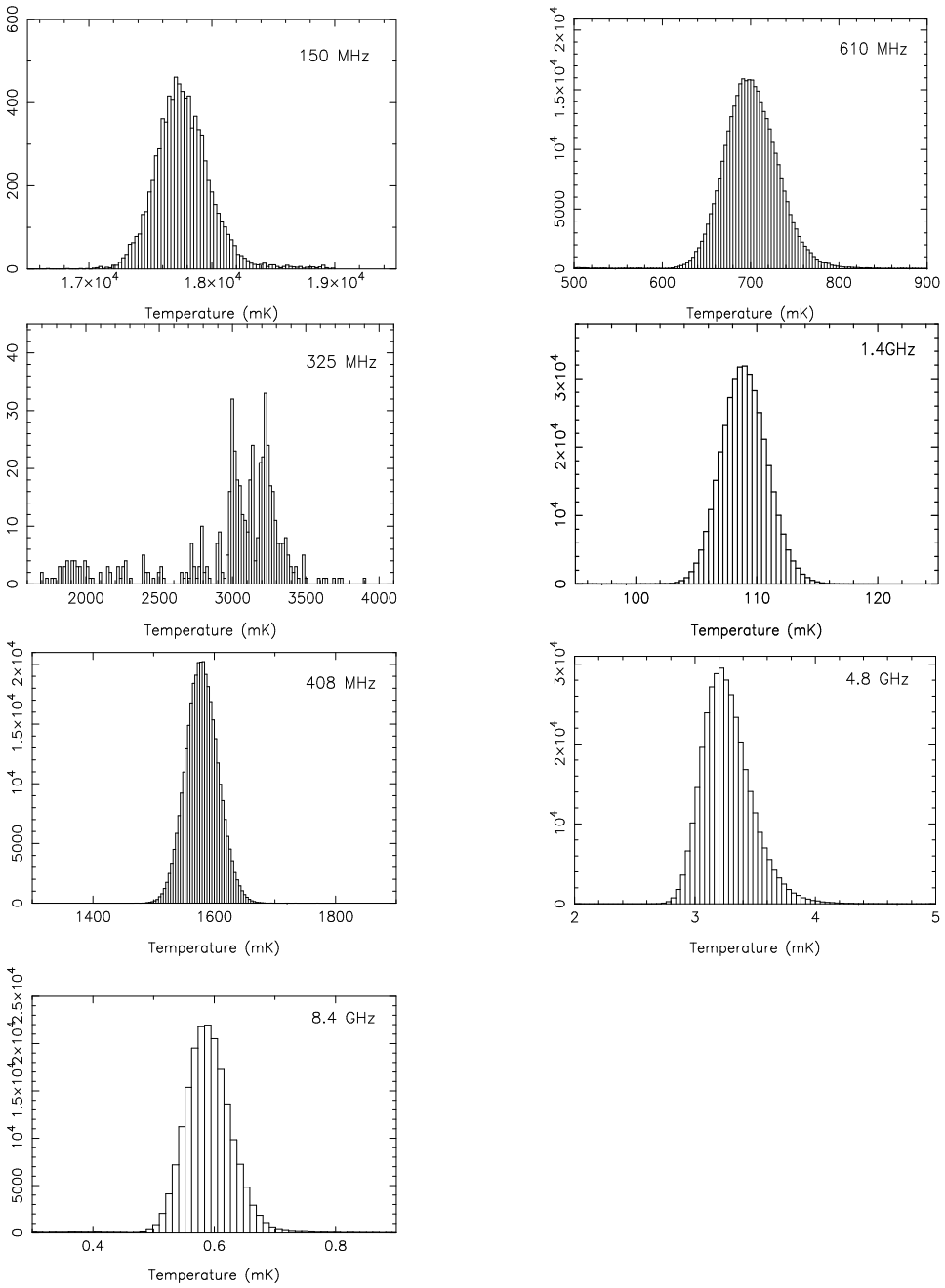

Figure 3.4: Histograms from the Markov chains at each frequency. The background temperature was computed at each step in the chain and binned. At most frequencies there is a well defined value of the CRB with an approximately Gaussian distribution, while this is less true at 325 MHz in particular.

values, e.g. at 408 MHz. However, there is a noticeable irregularity with the 325 MHz histogram. Because of the limited data available at 325 MHz, and with the peak area of contribution having little to no data, the histogram at this frequency does not have a well defined shape; the uncertainty is far from Gaussian.

3.3 Comparison with Previous Estimates

Over the years there have not been many estimates of the CRB made using source count data [14, 21, 38, 51, 63]. And even within this small list, the frequencies covered were rather limited and uncertainties not always quoted. It is important to see how our estimates compare with these previous estimates. Longair [38] gives a value for $T_{178} = 23 \pm 5$ K. Wall [63] lists estimates of $T_{408} = 2.6\,\mathrm{K}$, $T_{1.4} = 0.09\,\mathrm{K}$, and $T_{2.5} = 0.02$ K. Our results are in agreement with these earlier estimates to within $\pm\, 2\sigma$. The values for source contributions from Gervasi et al. (2009) tend to be a little higher than ours, the differences being traceable to choices made for the limits of integration and for the parameterized form for the fits.

The ARCADE 2 experiment reported an excess of emission beyond what we and others have estimated from source counts, with the excess largest at 3.4 GHz. We have also considered much lower frequencies in this paper than the 3.2 GHz detection limit of ARCADE 2. However, it is possible to calculate what temperatures would be expected using the best fit to the ARCADE 2 data:

$$T(\nu) = T_0 + A\left(\frac{\nu}{1\mathrm{GHz}}\right)^{\beta} \quad . \tag{3.4}$$

Here T_0 is the CMB base temperature, and the best fit values for the parameters are β = –2.56 and A = 1.06 [57]. Measurements from the TRIS experiment were performed at ν = 0.6, 0.82, and 2.5 GHz, and compared with the Gervasi et al. [21] source contribution calculations are within 3% at 0.6 GHz and 50% at 2.5 GHz

The quantities detected by or extrapolated from ARCADE 2, those estimated from counts by Gervasi et al. [21], the measurements from the TRIS experiment, as well as our current estimates are all shown in Fig. 3.5. Here it can be seen that the ARCADE 2 absolute measurements lie far above both source estimates and TRIS measurements, particularly at lower frequencies. Clearly, the excess

detected around 3 GHz would correspond to a large excess at lower frequencies if the power-law behaviour continued.

3.4 Systematic Errors

We have considered several possibilities for systematic errors in exploring whether our results might be compatible with those from the ARCADE 2 experiment. The first of these is possible bias from source clustering. This can be an issue when dealing with surveys covering small areas, where one might get more field-to-field variations than expected from Poisson errors. The two-point angular correlation function for NVSS and FIRST sources fits a power-law shape for separations up to at least 4° [3, 47]. From this angular correlation one can estimate the fractional variance of the counts [58]. This procedure was carried out by de Zotti et al. [11] and has been taken into account in the errors provided and used in our estimations.

Another effect that could influence our results is the fact that in some of the surveys used in our compilation the measurement frequency was slightly different from the nominal one, i.e. 5 GHz rather than 4.8 GHz. In such cases we scaled the original measurements to the nominal frequency using the assumed dependence of the source flux $S(\nu) \sim \nu^{-0.7}$. This correction results in negligible change in the derived fits.

An additional effect that could account for the difference in the background temperatures is the possibility that some surveys have somehow missed extended high-frequency emission blobs which could integrate up to the required amounts. This seems an unlikely option, as such structures would have to be on degree scales or larger to escape detection, and because if these structures have features above a certain brightness temperature then they would have been seen.

Other possible effects to take into consideration for the uncertainties include:

1. Calibration variations for different radio telescopes;

2. Inaccurate determination of completeness corrections at the faint end;

3. Contribution from diffuse emission from the Intergalactic Medium (IGM), Intercluster Medium (ICM), and the Warm-Hot Intergalactic Medium (WHIM);

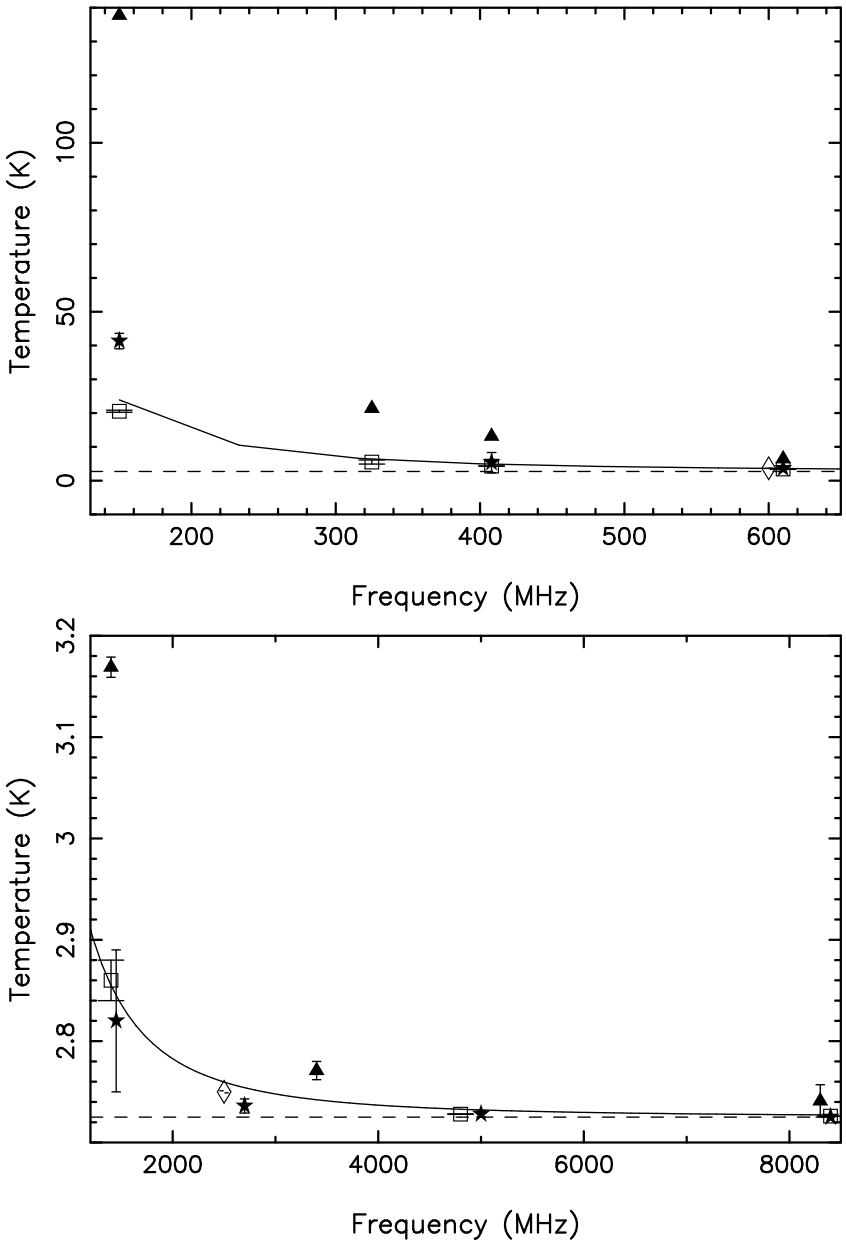

Figure 3.5: Integrated sky brightness temperature at each frequency from the estimates in this paper (open squares), Gervasi et al. [21] (stars), TRIS measurements (Zannoni et al. [69], diamonds), and ARCADE 2 measurements (Seiffert et al. [57], triangles). The solid line is our power law fit from Section 3.1. The dashed line at the bottom represents the CMB temperature at 2.7255 K [15].

4. Missing low surface brightness emission from extended objects that are either large, or sources with extended components, or sources that are not detected if source surface brightness extends to low values.

Singal et al. [60] provide a detailed discussion of items 3 and 4 as well as several other possibilities such as radio supernovae that could contribute to the CRB. We suspect that the most important effects are the first two items, particularly completeness at the faint end. Detailed discussion of these issues would require investigation of the raw data from the individual data sets and is beyond the scope of this thesis.

Chapter 4

Discussion

4.1 Investigation of a Faint 'Bump' in the Counts

At 1.4 GHz, where we have the most data, our estimated background temperature plus a CMB baseline is $2.83\,\mathrm{K} \pm 0.02\,\mathrm{K}$, while an extrapolation of the ARCADE 2 result gives $3.17\,\mathrm{K} \pm 0.01\,\mathrm{K}$ (error estimate from their measurement at 3.2 GHz). This corresponds to a difference that is nearly 17σ away from our estimate. It has been suggested that this could be explained through an extra population of faint radio galaxies, corresponding to a 'bump' in the Euclidean-normalized counts at flux densities near or below where the current data are petering out (see also Singal et al. [60]). We want to investigate how big this bump would need to be in order to explain the excess emission.

We carried out two separate approaches for modelling such a bump, the outcomes of which can be seen in Fig. 4.1. Our first approach is a simple extension of the current counts, with an upward trend below 10 μJy, but one not quite as steep as the best–fit line. To do this we simply added artificial data points past the lower flux density limit of the rest of the data in order to control the end behaviour of the fit line. We then investigated what was required to match the ARCADE 2 results. The solid line of Fig. 4.1 shows the results of this fitting. It is the best fit to the data, allowing for a moderate upward slope in the faint end. When integrated from 10^{-6}Jy the result is enough to account for the temperature reported by ARCADE 2.

Our second method involved choosing a simple parabola with fixed width of a

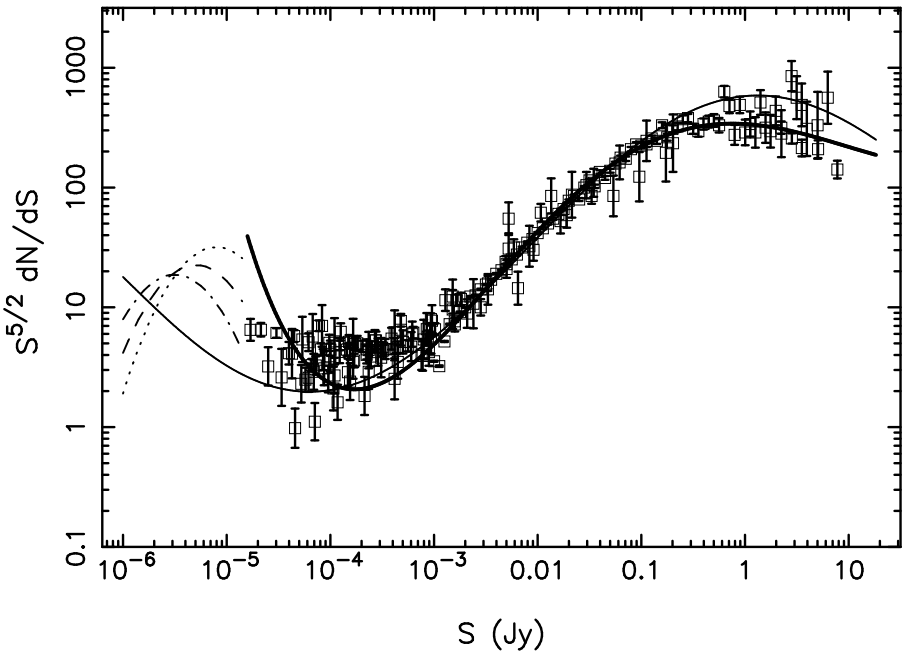

Figure 4.1: The 1.4 GHz source count data. The thin solid line gives the best fit to the data while having a moderate slope at the faint end and integrating to the necessary excess reported by ARCADE 2. The thick solid line is our best fit to the 1.4 GHz data from section 2.2. The other three lines are bumps peaking at 7.9 (dotted), 5.0 (dashed), and 3.1 (dot dash) μJy, which produce the background temperature necessary to match the ARCADE 2 results. On this plot the height of such a bump is proportional to $S_{\rm peak}^{1/2}$

decade in log-S and variable position for the peak, and running a Markov chain that fit the height parameter that would integrate to give the amount of excess emission needed to match the ARCADE 2 result. We found that the peak of the bump could be at flux densities as high as 8.0 μJy.

It is relatively easy to produce a bump big enough to account for the extra emission while still fitting the rest of the data reasonably well, with either method. However, we do know that any such bump is constrained by the observed IR background, through the IR-Radio correlation (see e.g. Haarsma and Partridge 26). This correlation will have to be taken into account in any modelling of this faint

flux density bump so as not to overproduce the IR background. This essentially requires any faint radio population to be quite IR faint compared with known galaxy types.

4.2 Preliminary Bump Investigation Using Stacking

The bumps modelled in the above section showed that the size of a faint flux-density bump was not unreasonable. Now follow up is needed to look for signs of such a population of faint radio sources. One way of doing this is through the technique of signal stacking.

The sources that may be causing the unexplained excess in radio emission are very faint, perhaps around 1 μJy. This is too faint to be detected individually by current surveys. To get around this fact we can use the technique of signal stacking, whereby we average the signal from sources at multiple locations that would otherwise be undetectable. This technique involves simply adding the flux density at multiple locations corresponding to source positions identified at other wavelengths, and taking the average. The great advantage of this technique is the gain in signal-to-noise ratio. Combining many sources reduces the random noise while maintaining the average level of the signal. This gain is at the expense of knowledge about the individual galaxies, but with carefully chosen criteria and a large enough sample it can reveal properties of galaxies below the noise and confusion limits.

We decided to try stacking onto the VLA 1.4 GHz image of the Great Observatories Origins Deep Survey North (GOODS–N) field. The GOODS–N field [12, 22] covers roughly 160 arcmin^2, centred on the Hubble Deep Field North [65]. Not only is this a very deep radio image but the field also has high resolution data available in the infrared (*Spitzer*), optical(*Hubble*/ACS), and X-ray (*Chandra*). We are also stacking onto a 610 MHz image from the GMRT of the GOODS–N field (Ivison et al. *in preparation*). The 610 MHz map can be used as a check for any signal which might be found at 1.4 GHz, since any signal at 1.4 GHz should presumably be stronger at 610 MHz.

We used the *HST*/ACS optical source catalogue from the GOODS–N field, which contains 32,048 sources in the b, v, i, and z bands. We also use *Spitzer*/IRAC

source catalogue which contains 19,438 sources at 3.6, 4.5, 5.8, and 8.0 μm. Using the positions of these sources with different brightness and colour cuts we are able to look for a faint signal that might otherwise not be seen.

Stacking onto radio maps has not been done nearly as often as stacking onto other wavelengths. This is because it is generally thought to present many difficulties due to the correlated noise of the images. However, many of these difficulties can be avoided with the realization that the technique is really just taking the covariance of the map with the stacking catalogue (see Marsden et al. [41] for a full discussion). Our method for stacking is to take the pixel value, in Jy beam^{-1}, of the radio map at the position of the catalogue sources, add up those values, and take the average, Fig. 4.2 shows an example. We also need to know the average of the radio map itself, so we add up all the pixel values and average those. This comes out to slightly higher than zero, 0.1 μJy and 2.9 μJy for the 1.4 GHz and 610 MHz maps respectively. The average of the maps must be subtracted from the source stacks to get a reliable result.

To obtain an estimate of the uncertainty in the stack signals we generate random catalogues, or catalogues of random positions, a thousand times, and look at the standard deviation of the distribution. The uncertainties are well described by Gaussian distributions and scale according to the map rms divided by the square root of the number of catalogue entries (see Fig. 4.3).

When considering what sources to stack we have to consider the potential characteristics of this population. We know that it must be faint, not just in the radio but also at other wavelengths. If it were bright in other wavebands it would most likely have been identified and studied by now. So when stacking, a magnitude or brightness limit must be imposed. As well, we can assume these objects are likely to lie at higher redshifts, $z > 1$, so when doing a colour cut, or difference in two wavebands, we can impose a restriction to look at the redder (or higher redshift) objects. Also, we do not expect there to be many of these objects detectable, perhaps around 100 objects (again, because otherwise it seems likely their existence would already have been discovered). So we are looking for just a hint of a fainter population.

Taking the above mentioned constraints into account, we simply try different combinations of colour cuts, with different magnitude limits, using the different

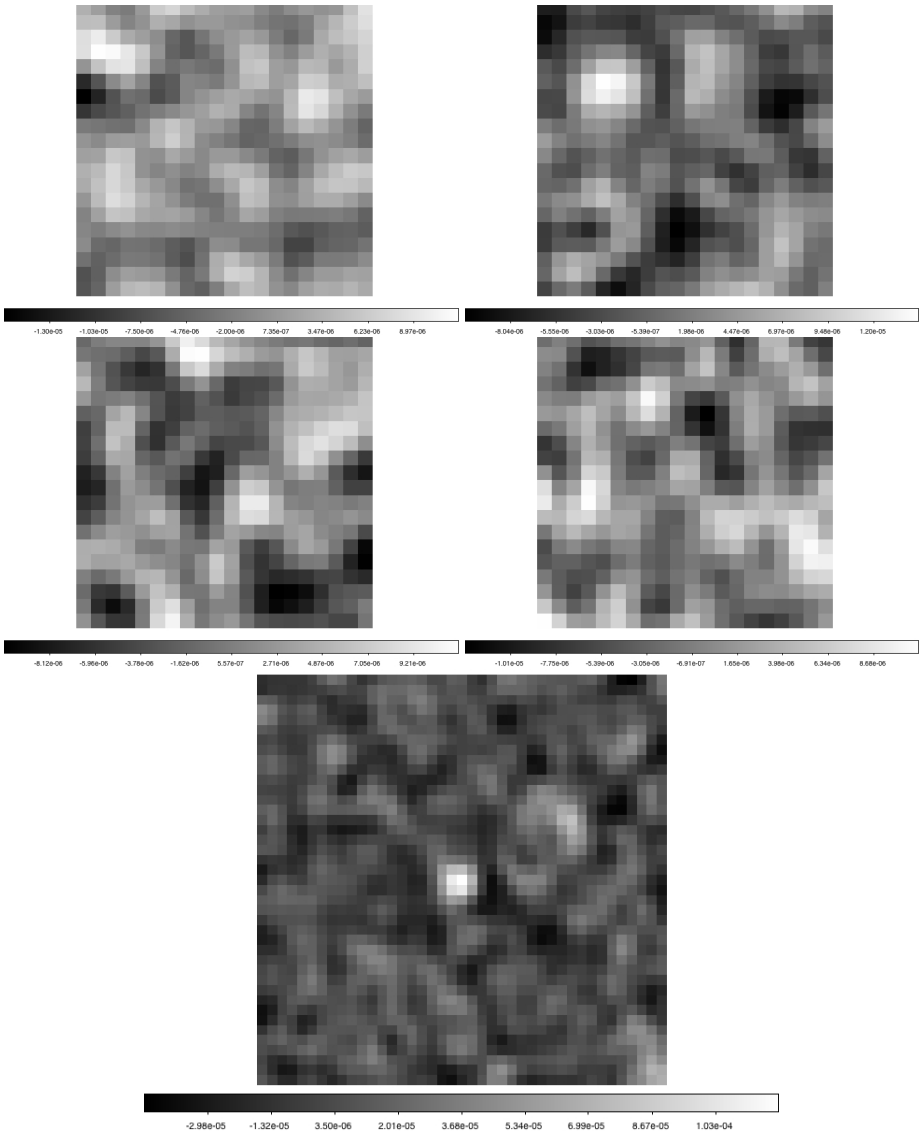

Figure 4.2: Four sample images from the 1.4 GHz VLA map, centred on pixel at RA and DEC of IRAC sources. Larger image at the bottom is a compilation of 40 individual images added together and then averaged, it is the stack. In the centre a bright source is visible indicating that the centre of the other images added together yields a bright source.

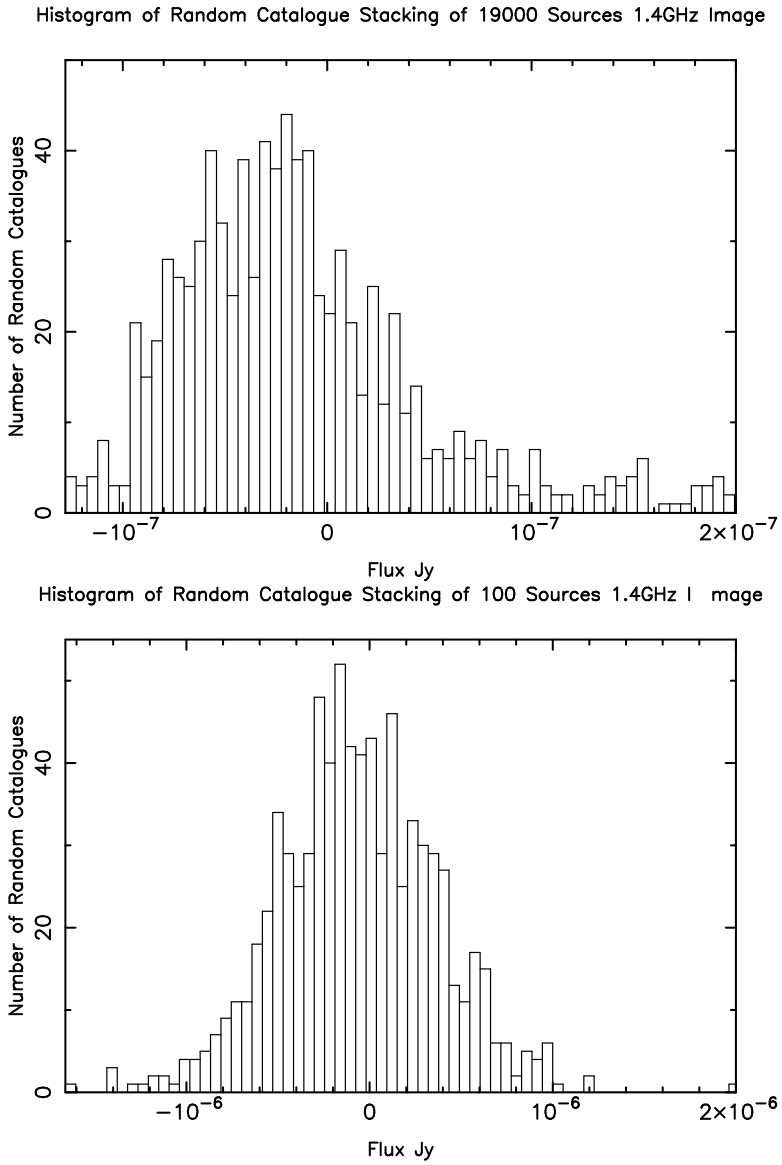

Figure 4.3: Two distributions from random catalogue stacking on the 1.4 GHz map. *Top*: distribution of random catalogues with 19,000 catalogue positions, which is essentially a sampling of the whole image. This is centred on zero, with a standard deviation of 0.092 μJy. *Bottom*: Distribution of random catalogues with 100 catalogue positions. The standard deviation here is 2.50 μJy. The smaller the number of catalogue entries gives a much broader distribution, which forms a more realistic comparison with the $\sim$100 object stacks.

catalogues and look for any sign of a signal that would indicate a population. In Fig. 4.4 the magnitude and colour of the catalogue sources are divided into bins and stacked. In this type of representation we can explore if there are any areas of strong signal to investigate further. The number of sources per bin varies, with around several hundred at the bright blue end (lower left) to only about 10 objects per bin at the red faint end (upper right).

These plots show there is a lot of variability between the different magnitude bins for the same colour bin, and vice versa. There is also some variability between the two radio maps. Usually if a source is bright at 1.4 GHz it should also be bright, or brighter, at 610 MHz. However, we can see that in some bins where the stack seems to have a strong signal in the 1.4 GHz image, it appears very weak in the 610 MHz image; this requires further investigation, to see if it is an effect of the how the maps were made or perhaps is just a result of the signal being too noisy at these flux density levels.

Nevertheless there are some hints of a possible population. Further investigation into the selections that look like they might have a significant stack signal is done by checking the ACS and IRAC images of the relevant sources. More specifically we can look to see if they are already identified in the literature as known AGN, star forming galaxies, etc., and we can check other information such as red shift, if known. At this point when investigating apparently strong signal areas, no known counterparts have been identified. Using the GOODS–N/NICMOS redshift catalogue some of the sources have been matched with redshift and it looks the as though those of interest lie primarily at $z > 1$, but with large photometric redshift uncertainties.

At this current stage the results from the this stacking analysis are inconclusive and require further work. The range of properties in Fig. 4.4 that appear to have a strong stacking signal may not be significant, because of low number statistics. The stacking work may yet yield some information about a new population of radio sources, or at least place new constraints on this possible population. We will continue this investigation until more concrete conclusions can be drawn.

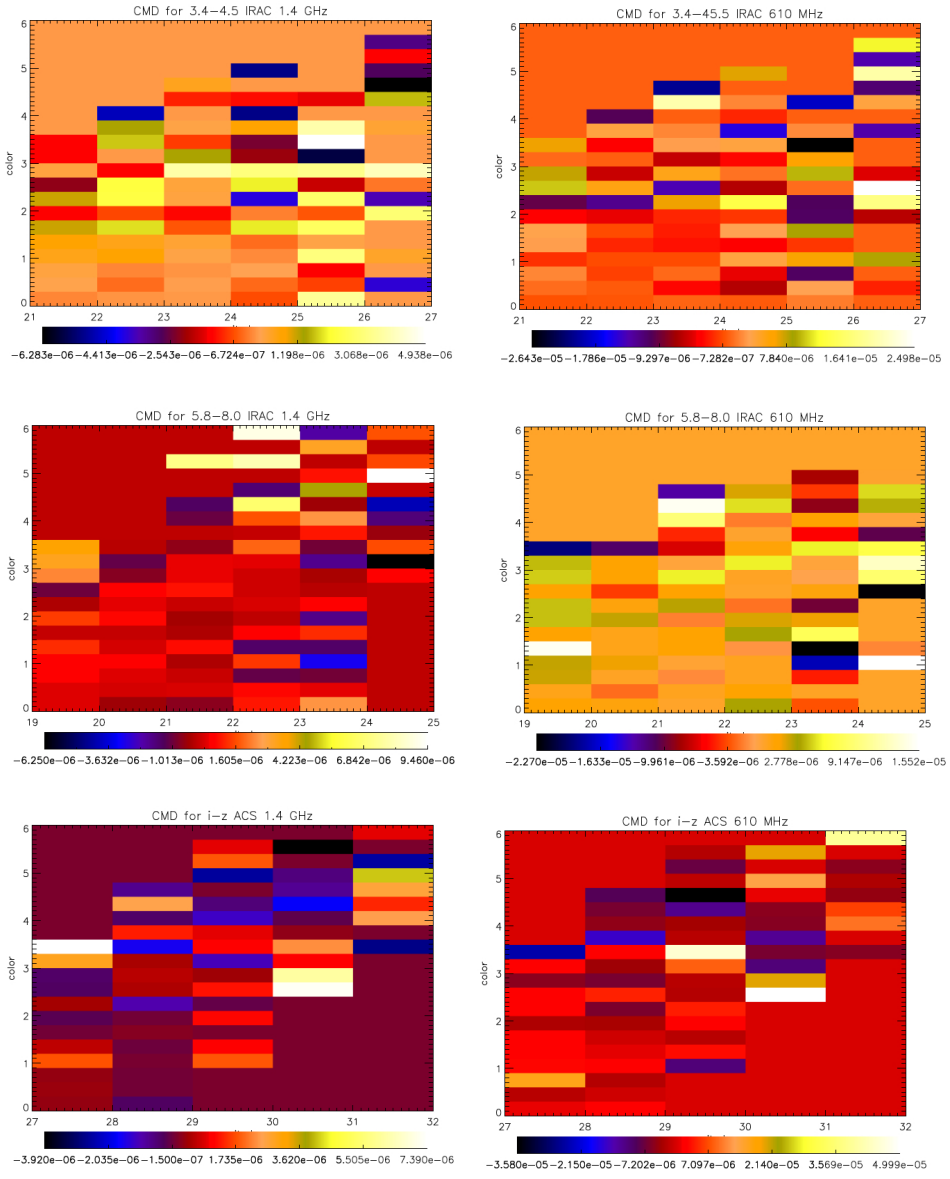

Figure 4.4: Colour magnitude diagrams for three colour cuts: IRAC 3.0–4.5 μm (top); 5.8–8.0 μm (middle), and ACS i–z (bottom). These are for the 1.4 GHz radio image (left) and 610 MHz image (right). The colour cut is divided into bins of 0.3. There are blank areas in the upper left and lower right, showing there are no objects that are bright and red and none that are very faint and blue. The number of sources per bin varies, with around several hundred at lower left to only about 10 objects per bin at the upper right.

Chapter 5

Conclusions

We used source count data from ν = 150 MHz, 325 MHz, 408 MHz, 610 MHz, 1.4 GHz, 4.8 GHz, and 8.4 GHz to evaluate the contribution from sources to the diffuse cosmic radio background. Polynomials were fit to the data and integrated to obtain lower bound estimates at each frequency for the sky brightness temperature. In addition, we also extrapolated our fits beyond the limits where data are available using reasonable assumptions for how the curves behave in those regions. We then used Monte Carlo Markov Chains to obtain estimates of the uncertainties of the temperature estimates at each frequency and also considered other possible sources of uncertainties that could affect the results.

Our estimates are considerably lower than the measurements of ARCADE 2, even when taking into account the uncertainties or extrapolations. We considered the possibility that the excess emission comes from a bump in the source counts in the μJy range at 1.4 GHz. We used modelling to see how large such a bump must be in order to obtain the necessary contribution to the background. We saw that a bump could exist in this range, peaking at fluxes as bright as 8 μJy, and could integrate up to the excess emission of $\pm$ 320 mK, with a height that is consistent with the data. We are in the process of searching for a signal from this population using stacking analysis, however, we have no conclusive results from the stacking at this time.

We still have no direct evidence that such a new population exists, and so further investigation into the faint end of the counts is needed. The final answer may

only be reached when source count data become available in the μJy range, perhaps in the era of the EVLA [50] and eventually the SKA Jackson [32].

In Section 4.1 several possible bump models were shown. These were modelled with simple parabolas to see if something that could integrate up to the necessary amount was reasonable. These bumps, however, have no physical grounding. We do not know if a population could reasonably exist that would produce a similar shape. One way to see if these bumps could physically exist is to use them to model the radio luminosity function of such a population and compare to luminosity functions from currently known populations. Depending on the results, this may also tell us about the possible evolution of this new population.

We are also hopeful that in the near future, most probably with the EVLA, we will obtain new deeper radio data that will allow for fainter source count estimates or investigation of this flux-density space with a $P(D)$, or probability of deflection, analysis (Scheuer [56]).

The ARCADE 2 data served as a major part of the motivation for the present work. Whether or not the indications of a high radio background turn out to be correct, an investigation of radio sources at the faintest possible flux densities will certainly provide interesting on galaxy evolution.

Bibliography

[1] D. R. Altschuler. A 5-GHz survey of radio sources. *Astron. Astrophys. Suppl. Ser.*, 65:267–281, Aug. 1986. → pages 7

[2] C. R. Benn, G. Grueff, M. Vigotti, and J. V. Wall. A deep radio/optical survey near the North Galactic Pole. I. The 5C12 catalogue. *MNRAS*, 200: 747–766, Aug. 1982. → pages 7

[3] C. Blake and J. Wall. Quantifying angular clustering in wide-area radio surveys. *MNRAS*, 337:993–1003, Dec. 2002. doi:10.1046/j.1365-8711.2002.05979.x. → pages 17

[4] M. Bondi, P. Ciliegi, G. Zamorani, L. Gregorini, G. Vettolani, P. Parma, H. de Ruiter, O. Le Fevre, M. Arnaboldi, L. Guzzo, D. Maccagni, R. Scaramella, C. Adami, S. Bardelli, M. Bolzonella, D. Bottini, and A. Cappi. The VLA-VIRMOS Deep Field. I. Radio observations probing the mu Jy source population. *Astronomy & Astrophysics*, 403:857–867, June 2003. doi:10.1051/0004-6361:20030382. → pages 6

[5] M. Bondi, P. Ciliegi, T. Venturi, D. Dallacasa, S. Bardelli, E. Zucca, R. M. Athreya, L. Gregorini, A. Zanichelli, O. Le Fèvre, T. Contini, B. Garilli, A. Iovino, S. Temporin, and D. Vergani. The VVDS-VLA deep field. III. GMRT observations at 610 MHz and the radio spectral index properties of the sub-mJy population. *Astronomy & Astrophysics*, 463:519–527, Feb. 2007. doi:10.1051/0004-6361:20066428. → pages 7

[6] M. Bondi, P. Ciliegi, E. Schinnerer, V. Smolčić, K. Jahnke, C. Carilli, and G. Zamorani. The VLA-COSMOS Survey. III. Further Catalog Analysis and the Radio Source Counts. *ApJ*, 681:1129–1135, July 2008. doi:10.1086/589324. → pages 7

[7] W. N. Brandt and G. Hasinger. Deep Extragalactic X-Ray Surveys. *Ann.Rev.Astr.Ap.*, 43:827–859, Sept. 2005. doi:10.1146/annurev.astro.43.051804.102213. → pages 1

[8] A. H. Bridle, M. M. Davis, E. B. Fomalont, and J. Lequeux. Flux densities, positions, and structures for a complete sample of intense radio sources at 1400 MHz. *A.J.*, 77:405–443, Aug. 1972. doi:10.1086/111301. → pages 7

[9] P. Ciliegi, R. G. McMahon, G. Miley, C. Gruppioni, M. Rowan-Robinson, C. Cesarsky, L. Danese, A. Franceschini, R. Genzel, A. Lawrence, D. Lemke, S. Oliver, J. Puget, and B. Rocca-Volmerange. A deep VLA survey at 20 CM of the ISO ELAIS survey regions. *MNRAS*, 302:222–244, Jan. 1999. doi:10.1046/j.1365-8711.1999.02103.x. → pages 7

[10] J. J. Condon and K. J. Mitchell. A deeper VLA survey of the alpha = 08h52m15s, delta = +17 deg 16 arcmin field. *A.J.*, 89:610–617, May 1984. doi:10.1086/113556. → pages 8

[11] G. de Zotti, M. Massardi, M. Negrello, and J. Wall. Radio and millimeter continuum surveys and their astrophysical implications. *Astronomy & Astrophysics Reviews*, 18:1–65, Feb. 2010. doi:10.1007/s00159-009-0026-0. → pages 6, 17

[12] M. Dickinson, C. Papovich, H. C. Ferguson, and T. Budavári. The Evolution of the Global Stellar Mass Density at 0¡z¡3. *ApJ*, 587:25–40, Apr. 2003. doi:10.1086/368111. → pages 22

[13] R. H. Donnelly, R. B. Partridge, and R. A. Windhorst. 6 centimeter radio source counts and spectral index studies down to 0.1 millijansky. *ApJ*, 321: 94–112, Oct. 1987. doi:10.1086/165618. → pages 7

[14] L. Feretti, C. Burigana, and T. A. Enßlin. Diffuse radio emission from the intracluster medium. *New Astronomy Reviews*, 48:1137–1144, Dec. 2004. doi:10.1016/j.newar.2004.09.025. → pages 1, 16

[15] D. J. Fixsen. The Temperature of the Cosmic Microwave Background. *ApJ*, 707:916–920, Dec. 2009. doi:10.1088/0004-637X/707/2/916. → pages vii, 18

[16] D. J. Fixsen, A. Kogut, S. Levin, M. Limon, P. Lubin, P. Mirel, M. Seiffert, J. Singal, E. Wollack, T. Villela, and C. A. Wuensche. ARCADE 2 Measurement of the Extra-Galactic Sky Temperature at 3-90 GHz. *ArXiv e-prints*, Jan. 2009. → pages 5

[17] E. B. Fomalont, K. I. Kellermann, J. V. Wall, and D. Weistrop. A deep 6-centimeter radio source survey. *Science*, 225:23–28, July 1984. doi:10.1126/science.225.4657.23. → pages 7

[18] E. B. Fomalont, K. I. Kellermann, R. B. Partridge, R. A. Windhorst, and E. A. Richards. The Microjansky Sky at 8.4 GHz. *A.J.*, 123:2402–2416, May 2002. doi:10.1086/339308. → pages 6, 7

[19] E. B. Fomalont, K. I. Kellermann, L. L. Cowie, P. Capak, A. J. Barger, R. B. Partridge, R. A. Windhorst, and E. A. Richards. The Radio/Optical Catalog of the SSA 13 Field. *Ap.J. (Suppl)*, 167:103–160, Dec. 2006. doi:10.1086/508169. → pages 7

[20] T. Garn, D. A. Green, J. M. Riley, and P. Alexander. A 610-MHz survey of the Lockman Hole with the Giant Metrewave Radio Telescope - I. Observations, data reduction and source catalogue for the central 5 deg^2. *MNRAS*, 387:1037–1044, July 2008. doi:10.1111/j.1365-2966.2008.13335.x. → pages 7

[21] M. Gervasi, A. Tartari, M. Zannoni, G. Boella, and G. Sironi. The Contribution of the Unresolved Extragalactic Radio Sources to the Brightness Temperature of the Sky. *ApJ*, 682:223–230, July 2008. doi:10.1086/588628. → pages vii, 3, 6, 16, 18

[22] M. Giavalisco, H. C. Ferguson, A. M. Koekemoer, and M. Dickinson. The Great Observatories Origins Deep Survey: Initial Results from Optical and Near-Infrared Imaging. , 600:L93–L98, Jan. 2004. doi:10.1086/379232. → pages 22

[23] P. C. Gregory, W. K. Scott, K. Douglas, and J. J. Condon. The GB6 Catalog of Radio Sources. *Ap.J. (Suppl)*, 103:427–+, Apr. 1996. doi:10.1086/192282. → pages 7

[24] G. Grueff. A Determination of the 408-MHZ Log N-Log from the b3 Radio Sources Catalogue. *Astronomy & Astrophysics*, 193:40–+, Mar. 1988. → pages 7

[25] C. Gruppioni, P. Ciliegi, M. Rowan-Robinson, L. Cram, A. Hopkins, C. Cesarsky, L. Danese, A. Franceschini, R. Genzel, A. Lawrence, D. Lemke, R. G. McMahon, G. Miley, S. Oliver, J. Puget, and B. Rocca-Volmerange. A 1.4-GHz survey of the southern European Large-Area ISO Survey region. *MNRAS*, 305:297–308, Apr. 1999. doi:10.1046/j.1365-8711.1999.02415.x. → pages 7

[26] D. B. Haarsma and R. B. Partridge. Radio Wavelength Constraints on the Sources of the Far-Infrared Background. , 503:L5+, Aug. 1998. doi:10.1086/311528. → pages 21

[27] S. E. G. Hales, J. E. Baldwin, and P. J. Warner. The 6C survey of radio sources. II - The zone delta = 30-51 deg, alpha = 08h30m-17h30m. *MNRAS*, 234:919–936, Oct. 1988. → pages 7

[28] M. G. Hauser and E. Dwek. The Cosmic Infrared Background: Measurements and Implications. *Ann.Rev.Astr.Ap.*, 39:249–307, 2001. doi:10.1146/annurev.astro.39.1.249. → pages 1

[29] B. Henkel and R. B. Partridge. Completing the Counts of Radio Sources at 8.5 GHz. *ApJ*, 635:950–958, Dec. 2005. doi:10.1086/497588. → pages 7

[30] A. M. Hopkins, J. Afonso, B. Chan, L. E. Cram, A. Georgakakis, and B. Mobasher. The Phoenix Deep Survey: The 1.4 GHz Microjansky Catalog. *A.J.*, 125:465–477, Feb. 2003. doi:10.1086/345974. → pages vi, 4, 6, 7

[31] E. Ibar, R. J. Ivison, A. D. Biggs, D. V. Lal, P. N. Best, and D. A. Green. Deep multi-frequency radio imaging in the Lockman Hole using the GMRT and VLA - I. The nature of the sub-mJy radio population. *MNRAS*, 397: 281–298, July 2009. doi:10.1111/j.1365-2966.2009.14866.x. → pages 7

[32] C. A. Jackson. Deep radio continuum studies with the SKA: evolution of radio AGN populations. *New Astronomy Reviews*, 48:1187–1193, Dec. 2004. doi:10.1016/j.newar.2004.09.023. → pages 29

[33] J. K. Katgert. A catalogue of sources found at 610 MHz with the Westerbork synthesis radio telescope - Source counts and spectral index distributions. *Astronomy & Astrophysics*, 73:107–112, Mar. 1979. → pages 7

[34] P. Katgert, M. J. A. Oort, and R. A. Windhorst. The WSRT 1.4 GHz amalgamated source counts. *Astronomy & Astrophysics*, 195:21–24, Apr. 1988. → pages 6

[35] H. Kuehr, A. Witzel, I. I. K. Pauliny-Toth, and U. Nauber. A catalogue of extragalactic radio sources having flux densities greater than 1 Jy at 5 GHz. *Astron. Astrophys. Suppl. Ser.*, 45:367–430, Sept. 1981. → pages 7

[36] G. Lagache, J. Puget, and H. Dole. Dusty Infrared Galaxies: Sources of the Cosmic Infrared Background. *Ann.Rev.Astr.Ap.*, 43:727–768, Sept. 2005. doi:10.1146/annurev.astro.43.072103.150606. → pages 1

[37] A. Lewis and S. Bridle. Cosmological parameters from CMB and other data: A Monte Carlo approach. *Phys. Rev.D*, 66(10):103511–+, Nov. 2002. doi:10.1103/PhysRevD.66.103511. → pages 7, 13

[38] M. S. Longair. On the interpretation of radio source counts. *MNRAS*, 133: 421–+, 1966. → pages 1, 16

[39] M. S. Longair and R. A. Sunyaev. The Origin of the X-ray Background. *Ap.J. (Letters)*, 4:65–+, 1969. → pages 1

[40] P. Madau and L. Pozzetti. Deep galaxy counts, extragalactic background light and the stellar baryon budget. *MNRAS*, 312:L9–L15, Feb. 2000. doi:10.1046/j.1365-8711.2000.03268.x. → pages 1

[41] G. Marsden, P. A. R. Ade, J. J. Bock, E. L. Chapin, M. J. Devlin, S. R. Dicker, M. Griffin, J. O. Gundersen, M. Halpern, P. C. Hargrave, D. H. Hughes, J. Klein, P. Mauskopf, B. Magnelli, L. Moncelsi, C. B. Netterfield, H. Ngo, L. Olmi, E. Pascale, G. Patanchon, M. Rex, D. Scott, C. Semisch, N. Thomas, M. D. P. Truch, C. Tucker, G. S. Tucker, M. P. Viero, and D. V. Wiebe. BLAST: Resolving the Cosmic Submillimeter Background. *ApJ*, 707:1729–1739, Dec. 2009. doi:10.1088/0004-637X/707/2/1729. → pages 23

[42] M. M. McGilchrist, J. E. Baldwin, J. M. Riley, D. J. Titterington, E. M. Waldram, and P. J. Warner. The 7c Survey of Radio Sources at 151-MHZ - Two Regions Centred at Ra: 10H28M Dec: 41DEG and Ra: 06H28M Dec: 45DEG. *MNRAS*, 246:110–+, Sept. 1990. → pages 7

[43] N. A. Miller, E. B. Fomalont, K. I. Kellermann, V. Mainieri, C. Norman, P. Padovani, P. Rosati, and P. Tozzi. The VLA 1.4 GHz Survey of the Extended Chandra Deep Field-South: First Data Release. *Ap.J. (Suppl)*, 179: 114–123, Nov. 2008. doi:10.1086/591054. → pages 7

[44] K. J. Mitchell and J. J. Condon. A confusion-limited 1.49-GHz VLA survey centered on alpha = 13 H 00 M 37 s, delta = + 30 deg 34 arcmin. *A.J.*, 90: 1957–1966, Oct. 1985. doi:10.1086/113899. → pages 7

[45] D. Moss, N. Seymour, I. M. McHardy, T. Dwelly, M. J. Page, and N. S. Loaring. A deep Giant Metre-wave Radio Telescope 610-MHz survey of the 1^H XMM-Newton/Chandra survey field. *MNRAS*, 378:995–1006, July 2007. doi:10.1111/j.1365-2966.2007.11842.x. → pages 7

[46] M. J. A. Oort, W. J. G. Steemers, and R. A. Windhorst. A deep 92 CM survey of the Lynx area. *Astron. Astrophys. Suppl. Ser.*, 73:103–123, Apr. 1988. → pages 7

[47] R. A. Overzier, H. J. A. Röttgering, R. B. Rengelink, and R. J. Wilman. The spatial clustering of radio sources in NVSS and FIRST; implications for galaxy clustering evolution. *Astronomy & Astrophysics*, 405:53–72, July 2003. doi:10.1051/0004-6361:20030527. → pages 17

[48] F. N. Owen and G. E. Morrison. The Deep Swire Field. I. 20 cm Continuum Radio Observations: A Crowded Sky. *A.J.*, 136:1889–1900, Nov. 2008. doi:10.1088/0004-6256/136/5/1889. → pages 7

[49] I. I. K. Pauliny-Toth, H. Steppe, and A. Witzel. A deep survey of selected regions for extragalactic sources at 4.85 GHz. *Astronomy & Astrophysics*, 85:329–331, May 1980. → pages 7

[50] R. A. Perley, C. J. Chandler, B. J. Butler, and J. M. Wrobel. The Expanded Very Large Array: A New Telescope for New Science. , 739:L1+, Sept. 2011. doi:10.1088/2041-8205/739/1/L1. → pages 29

[51] G. G. Pooley and M. Ryle. The extension of the number-flux density relation for radio sources to very small flux densities. *MNRAS*, 139:515–+, 1968. → pages 1, 16

[52] I. Prandoni, P. Parma, M. H. Wieringa, H. R. de Ruiter, L. Gregorini, A. Mignano, G. Vettolani, and R. D. Ekers. The ATESP 5 GHz radio survey. I. Source counts and spectral index properties of the faint radio population. *Astronomy & Astrophysics*, 457:517–529, Oct. 2006. doi:10.1051/0004-6361:20054273. → pages 6

[53] M. T. Ressell and M. S. Turner. The Grand Unified Photon Spectrum: A Coherent View of the Diffuse Extragalactic Background Radiation. *Comments on Astrophysics*, 14:323–+, 1990. → pages 1

[54] E. A. Richards. The Nature of Radio Emission from Distant Galaxies: The 1.4 GHZ Observations. *ApJ*, 533:611–630, Apr. 2000. doi:10.1086/308684. → pages 7

[55] J. G. Robertson. An all-sky catalogue of strong radio sources at 408 MHz. *Australian Journal of Physics*, 26:403–+, June 1973. → pages 7

[56] P. A. G. Scheuer. A statistical method for analysing observations of faint radio stars. *Proceedings of the Cambridge Philosophical Society*, 53: 764–773, 1957. doi:10.1017/S0305004100032825. → pages 29

[57] M. Seiffert, D. J. Fixsen, A. Kogut, S. M. Levin, M. Limon, P. M. Lubin, P. Mirel, J. Singal, T. Villela, E. Wollack, and C. A. Wuensche. Interpretation of the Extragalactic Radio Background. *ArXiv e-prints*, Jan. 2009. → pages vii, 5, 16, 18

[58] M. Seldner and P. J. E. Peebles. Clustering of Radio Sources in the 4C Catalog. In *Bulletin of the American Astronomical Society*, volume 12 of *Bulletin of the American Astronomical Society*, pages 471–+, Mar. 1980. → pages 17

[59] N. Seymour, T. Dwelly, D. Moss, I. McHardy, A. Zoghbi, G. Rieke, M. Page, A. Hopkins, and N. Loaring. The star formation history of the Universe as revealed by deep radio observations. *MNRAS*, 386:1695–1708, May 2008. doi:10.1111/j.1365-2966.2008.13166.x. → pages 7

[60] J. Singal, Ł. Stawarz, A. Lawrence, and V. Petrosian. Sources of the radio background considered. *MNRAS*, pages 1458–+, Sept. 2010. doi:10.1111/j.1365-2966.2010.17382.x. → pages 5, 8, 19, 20

[61] S. K. Sirothia, M. Dennefeld, D. J. Saikia, H. Dole, F. Ricquebourg, and J. Roland. 325-MHz observations of the ELAIS-N1 field using the Giant Metrewave Radio Telescope. *MNRAS*, 395:269–281, May 2009. doi:10.1111/j.1365-2966.2009.14317.x. → pages 6, 7

[62] T. Vernstrom, D. Scott, and J. V. Wall. Contribution to the diffuse radio background from extragalactic radio sources. *MNRAS*, 415:3641–3648, Aug. 2011. doi:10.1111/j.1365-2966.2011.18990.x. → pages 5

[63] J. V. Wall. The extragalactic radio source background. In S. Bowyer & C. Leinert, editor, *The Galactic and Extragalactic Background Radiation*, volume 139 of *IAU Symposium*, pages 327–332, 1990. → pages 1, 16

[64] R. L. White, R. H. Becker, D. J. Helfand, and M. D. Gregg. A Catalog of 1.4 GHz Radio Sources from the FIRST Survey. *ApJ*, 475:479–+, Feb. 1997. doi:10.1086/303564. → pages 7

[65] R. E. Williams, B. Blacker, M. Dickinson, W. V. D. Dixon, H. C. Ferguson, A. S. Fruchter, M. Giavalisco, R. L. Gilliland, I. Heyer, R. Katsanis, Z. Levay, R. A. Lucas, D. B. McElroy, L. Petro, M. Postman, H. Adorf, and R. Hook. The Hubble Deep Field: Observations, Data Reduction, and Galaxy Photometry. *A.J.*, 112:1335–+, Oct. 1996. doi:10.1086/118105. → pages 22

[66] R. A. Windhorst, G. K. Miley, F. N. Owen, R. G. Kron, and D. C. Koo. Sub-millijansky 1.4 GHz source counts and multicolor studies of weak radio galaxy populations. *ApJ*, 289:494–513, Feb. 1985. doi:10.1086/162911. → pages 8

[67] R. A. Windhorst, E. B. Fomalont, R. B. Partridge, and J. D. Lowenthal. Microjansky source counts and spectral indices at 8.44 GHz. *ApJ*, 405: 498–517, Mar. 1993. doi:10.1086/172382. → pages 7

[68] J. M. Wrobel and S. W. Krause. Counts of serendipitous 6 centimeter sources in E/S0 galaxy fields. *ApJ*, 363:11–20, Nov. 1990. doi:10.1086/169315. → pages 7

[69] M. Zannoni, A. Tartari, M. Gervasi, G. Boella, G. Sironi, A. De Lucia, A. Passerini, and F. Cavaliere. TRIS. I. Absolute Measurements of the Sky Brightness Temperature at 0.6, 0.82, and 2.5 GHz. *ApJ*, 688:12–23, Nov. 2008. doi:10.1086/592133. → pages vii, 3, 18